

Characterization of $\text{Bi}_{1.5}\text{Sb}_{0.5}\text{Te}_{1.8}\text{Se}_{1.2}$ nanoflakes

Thomas Klijnsma & Joris Voerman

August 2, 2012

Summary

This report describes the measurements performed on $\text{Bi}_{1.5}\text{Sb}_{0.5}\text{Te}_{1.8}\text{Se}_{1.2}$ (BSTS). The goal of this research is to determine the qualities of BSTS as a topological insulator. A topological insulator is a material that is insulating in the bulk, but conducting on the surface. For BSTS, the magnetoresistance and Hall resistance are researched as a function of temperature and magnetic field, and various other properties as a function of temperature. By characterizing the weak antilocalization in BSTS under a variety of angles and the use of very thin flakes, it is likely that surface states are observed.

Contents

1	Introduction	3
2	Theoretical Aspects	4
2.1	Topological Insulators	4
2.2	Landau Quantization and Shubnikov-de Haas oscillations	7
2.3	Weak antilocalization	8
3	Experimental Methods	12
3.1	Sample production	12
3.2	Measurements	12
4	Results	16
5	Conclusions	28

Chapter 1

Introduction

Topological insulators have gained immense interest of the scientific world in the past few years. Ever since the TU Delft published their paper on Majorana fermions, the whole world has heard about these elusive particles. In the search of these Majorana fermions complex devices, containing topological insulators (TI's), have to be made. The first two-dimensional TI, HgTe, has been discovered and characterized in 2007 [1]. A few years later three-dimensional structures were shown to be topological insulators, e.g. Bi₂Se₃, Bi₂Te₃ and Sb₂Te₃ [16]. In this report the material of interest is Bi_{1.5}Sb_{0.5}Te_{1.8}Se_{1.2}, or BSTS for short. This material should show a significant surface conductance and relatively low bulk conductance [14]. The goal is to characterize BSTS flake samples and observe the surface states that contain the interesting properties of a topological insulator. The required theory and experimental methods will be explained briefly in chapter 2 and 3. This is followed by the results, discussion and conclusion to the research.

Chapter 2

Theoretical Aspects

2.1 Topological Insulators

A topological insulator is essentially a crystal that has an insulating bulk and a conducting surface. They have been theoretically predicted in the 80's, but it wasn't until 2007 that M. Konig et al. demonstrated the effect in HgTe [1]. Topological insulators are often referred to as Quantum Spin Hall (QSH) insulators, which is a variation of the Quantum Hall Effect (QHE). When a conducting sheet is placed in a perpendicular magnetic field the trajectories of the free charge carriers are bent into circular orbits. These orbits are not to be confused with the regular orbits of bound electrons around the nucleus. This effect is illustrated in figure 2.1 below.

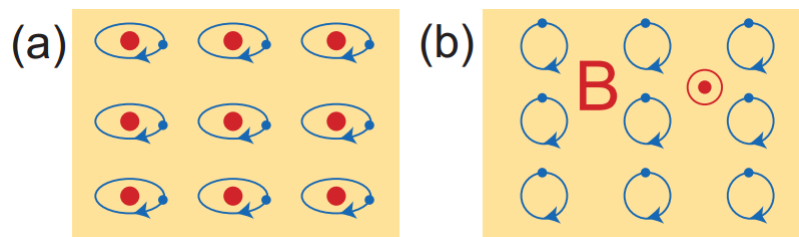


Figure 2.1: a) Electron orbits around their nuclei. b) electron orbits due to the perpendicular B-field (QHE) adapted from [2]

From figure 2.1 a) it can be seen that the electrons orbiting a nucleus do not contribute to the conductivity of the material. After a period of time the charge has not moved at all. And a moving charge is defined as the current. For the same reason the circular orbits in figure 2.1 b) do not contribute to a current. This parallel, however, ends at the edge of the crystal. The free charge carriers at the edge of the crystal are unable to form complete orbits and thus only form half orbits. This effect leads to a conducting outer edge of the crystal and is shown in figure 2.2.

Now that the conducting edge state has been made with the QHE, the step to QSH can be made. The Quantum Spin Hall effect is essentially the QHE without an externally

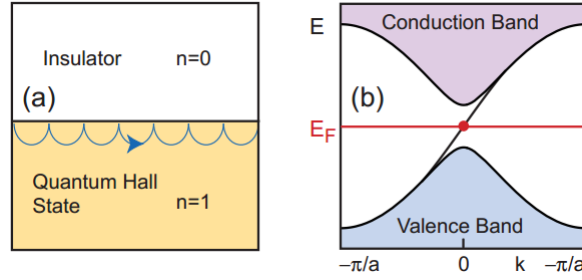


Figure 2.2: Quantum Hall Effect at the edge (insulator can be regarded as vacuum) adapted from [2]

applied magnetic field. Even though there is no external magnetic field, the electrons still experience a magnetic field due to the spin-orbit coupling (SOC)[3]. Typically for heavier elements (e.g. Hg, Te, Bi) this SOC is larger than for other atoms, which explains why only certain materials are TIs. The QSH effect separates the two conducting channels, which were present in the QHE state, into four. Both the upper and the lower side are separated into spin up and spin down. One may see the QSH effect as two copies of the QHE [4]. This effect is illustrated in figure 2.3.

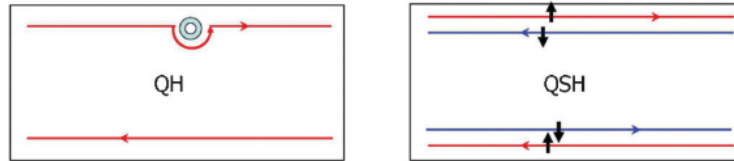


Figure 2.3: left: two edge states for QHE. right: 2x2 edge states for QSH. adapted from [4]

The right side of figure 2.3 shows that each side of the TI has both a backward and a forward moving lane. Scattering however of these lanes is prohibited due to destructive interference. When a charge carrier is reflected by an impurity in the crystal it can reflect 'clockwise' and 'counterclockwise' (see figure 2.4). For the clockwise rotation the spin, which is linked to the direction of the movement, is π . By the same logic the counterclockwise rotation rotates the spin by $-\pi$. The total rotation between the two waves is therefore $\pi - (-\pi) = 2\pi$. Due to what is known as the Berry phase, a spin-1/2 particle picks up a negative sign when it rotates by 2π [3]. These two waves will then destructively interfere very much like light waves. Because of this effect in a conducting state, the spin is locked to momentum [13]. The described interference also leads to weak antilocalization (see chapter 2.3)

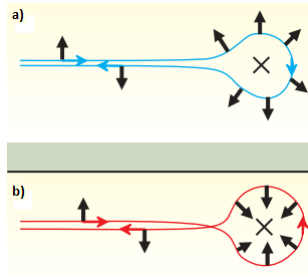


Figure 2.4: a) clockwise scattering, b) counterclockwise backscattering. adapted from [13]

Topology

So far the word 'topology' hasn't been covered at all. Topology is a field of mathematics concerned with the properties of objects under deformation [10]. Objects that can be twisted, pushed and bent into each other are topologically equal. For example a football and a dustbin are topologically equal, because one would only have to push down on the ball to make it bin-shaped. There is, however, a limit to what one can do with these objects. It is not allowed to poke holes into the object or to close holes. This means that a ring and ball are topologically different. The physical equivalent of this can be found in the bandgap of a system. One can shift the conduction and valence band around and still have the same topology. Closing, or opening, a bandgap is not allowed and leads to a new topological class. Figure 2.5 illustrates this. The system with the S band as conduction and P as valence band is topologically different from the system with P as conduction and S as valence band. When these two systems are brought together there *must* be a place where the bands cross and the bandgap is closed. And when bandgap closes there must be conduction. When it opens again the conduction disappears and we are left with an insulator. This shifting of the S and

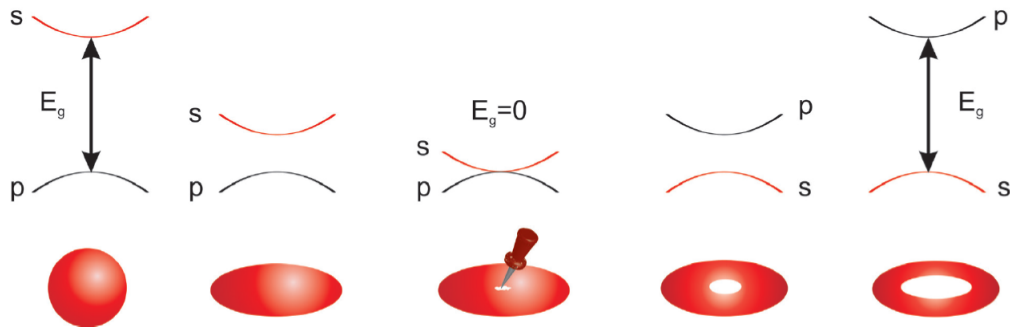


Figure 2.5: Left: S-conductance, P-valence. Right: P-conductance, S-valence. middle: Bandgap closes. the sphere and ring relate this to topology [8]

P band is caused by a phenomenon known as Spin-orbit coupling (SOC)[3]. From the

Pauli principle we can see that every energy state can have 2 electrons (one spin up and one spin down). This spin-momentum couples with the orbit, angular momentum, making a small correction to the energy levels of these two electrons. In some crystals this effect is strong enough to shift the bands past one another, creating a band diagram like the one shown in figure 2.5.

2.2 Landau Quantization and Shubnikov-de Haas oscillations

As mentioned in the previous paragraph, the essential property of a TI is the insulating bulk and conducting surface. In order to determine the applicability of BSTS as a TI it is necessary to observe the surface states in transport measurements. There are multiple ways to do this, two of which are described in this paragraph.

The first method of showing surface states is by measuring Shubnikov-de Haas (SdH) oscillations. These are oscillations in the conductance as a function of the applied magnetic field. SdH oscillations are typically seen at high magnetic fields ($> 3\text{T}$) and low temperatures ($< 20\text{K}$). These oscillations are caused by what is known as Landau quantization. The Landau quantization describes what happens to charged particles in a magnetic field. The particle trajectories will be bent into circles or cyclotron orbits. As is known from basic quantum mechanics, the wave function at one point must be the same as the wave function at that point $+ 2\pi$. In other words: the orbit has to fit to itself in order to make a circle. This creates allowed and disallowed energies for the particles. The energies that the charged particles can get from the magnetic field are thus quantized[5]. This creates peaks in the density of states (DOS). Theoretically these are delta peaks. The Landau quantization is shown in figure 2.6.

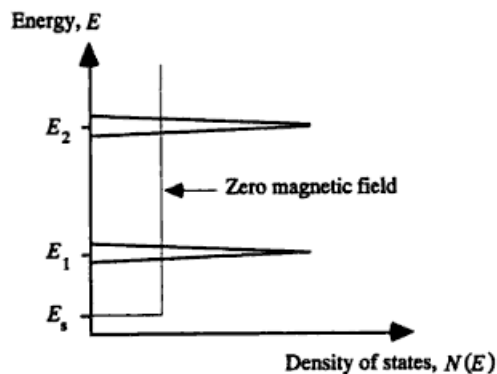


Figure 2.6: Density of States with Landau Quantization. [6]

The Landau quantization gives rise to a phenomenon known as Shubnikov-de Haas oscillations. The shifting of the Landau levels due to the magnetic field, gives rise to an overlap of the Fermi energy with either a high or a low density of states. Accordingly,

this leads to an oscillation in resistance [5]. This is illustrated in figure 2.7.

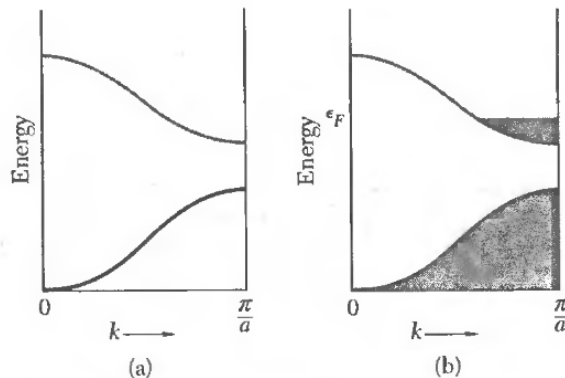


Figure 2.7: a) No states at E_f , insulator. b) States at E_f , metal. Adapted from [7]

The size of a Landau level, i.e. how many charge carriers can occupy the same energy level, is dependent on the magnetic field. The size of the Landau level is $\frac{2eB}{h}$ [6]. Thus by varying the magnetic field the Landau levels shift and sometimes cross the Fermi energy level. When this happens the conductance increases greatly. It falls off again when the Landau levels shift away from the Fermi energy. This gives rise to oscillations in the conductance, which we call Shubnikov-de Haas oscillations.

SdH-oscillations have an interesting and useful feature, by which they can be verified. The maxima in the resistance are related by $\frac{1}{B}$ [6]. The oscillations can be used to identify surface states [8] by rotating the sample in the magnetic field. The part of B that is perpendicular to the surface is dependent on the angle by $B_{\perp} = B \cos \theta$. And as before, the size of a Landau level is a function of the size of the magnetic field. The maxima of the oscillations in the resistance will thus shift in relation to the angle, which proves that there is a surface state present.

2.3 Weak antilocalization

A further analysis regarding the nature of the conductance in a topological insulator may be made with weak antilocalization. To understand this effect it is necessary to first understand weak localization, and it will turn out the two effects are very much alike. Consider an electron at position $r = 0$ and time $t = 0$, diffusing with the Fermi velocity v_f and the mean free path $l = v_f \tau$, τ being the average time between two elastic scattering events. After time $t \gg \tau_{\phi}$ (the time between two inelastic scatterings, thus changing the phase of the electron), the probability to find this electron at position r equals [9].

$$p(r, t) = (4\pi Dt)^{d/2} e^{-\frac{r^2}{4Dt}} \quad (2.1)$$

with the constraints:

$$\int p(r, t) dr = 1, \quad r^2 = \sum x_i^2 \quad (2.2)$$

Here D is the diffusion coefficient, defined as $\frac{lv_f}{d}$, and d is the dimensionality of the space in which diffusion takes place, in other words, the dimensionality of the system in which conductance is existent. With these definitions, consider an electron at $r = 0$, and $t = t$. The electron has, after time t , returned to its initial position, thus in a loop.

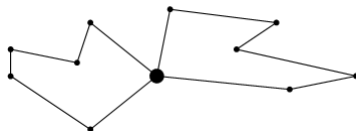


Figure 2.8: Two possible loops with 5 elastic scattering events, thus $t = 6\tau$ before the electron has returned to its initial position

Consider a loop with a certain number of scattering events. Note that the probability of an electron going through this loop one way equals the probability of an electron going through the loop in the opposite direction (clockwise and counter-clockwise, so to speak). The wave function in this loop would be described as the sum of the wave functions of both directions:

$$A_1\psi_1(r)\phi_1(t) + A_2\psi_2(r)\phi_2(t) \quad (2.3)$$

Classically, the contributions of both wave functions would be added separately to the total probability: $A_1^2 + A_2^2 = A^2 + A^2 = 2A^2$. In quantum mechanics however, the phase remains correlated until an inelastic scattering event occurs. Thus, for $t < \tau_\phi$, the wave functions can be added together since the wave functions of the electrons are still coherent. In that case, $[A_1 + A_2]^2 = A_1^2 + A_2^2 + 2|A_1A_2| = 4A^2$. The probability $p(r, t)$ is thus peaked at $r = 0$, with a probability twice as high as classically expected. The width of this peak is determined by the uncertainty principle.

Physically, this means that electrons are more likely to be at their initial position, or, differently stated, are less eager to move around. Thus, a heightened resistance is observed.

Strong spin-orbit coupling and the Berry phase

Strong spin-orbit coupling has a remarkable effect on the localization effect. From an electrons perspective, there is a magnetic field present in materials with high spin-orbit coupling [3].

$$B = \frac{1}{4\pi e_0} \frac{e}{mc^2 r^3} L \quad (2.4)$$

When an electron returns to its initial position through a loop, its spin has rotated by π , and $-\pi$ for the other way around. The total difference in spin rotation is thus π

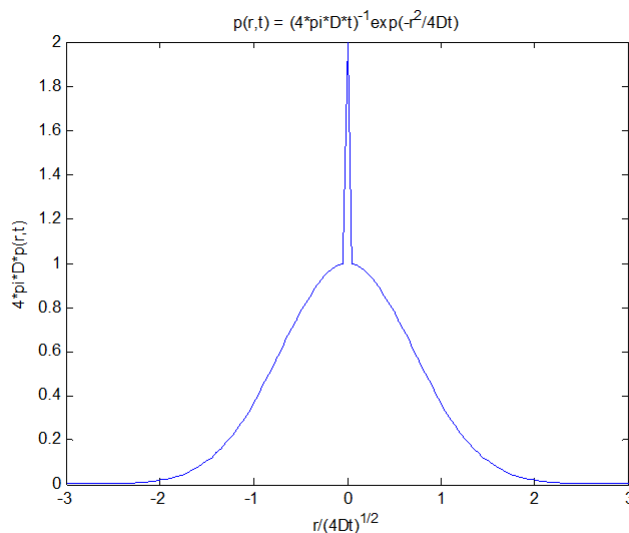


Figure 2.9: Peak due to weak localization
adapted from [9]

- $(-\pi) = 2\pi$. When spin rotates in a magnetic field, a somewhat obscure phenomenon occurs: its phase is shifted by exactly half of the spin rotation. This phase is called the Berry phase. In this particular case, the 2π spin rotation results in a phase difference of π , or, more intuitively, a minus sign [10]. Instead of constructive interference, there is now destructive interference due to spin-orbit coupling. Physically this results in the exact opposite of weak localization: the electron is now less likely to return to its initial position, which results in a lower resistance

Destroying (anti)localization with a magnetic field

Both localization and antilocalization are realized because of interference at the initial position of the electron. When a phase difference between the two wave functions is introduced from outside the sample, the interference is broken, and the localization or antilocalization is destroyed. Provoking an additional phase difference is easily done by applying an external magnetic field. For weak antilocalization, the dependence of the additional conductance on the applied magnetic field is provided by the Hikami-Larkin-Nagaoka formula [11].

$$\Delta\sigma = \frac{\alpha e^2}{h\pi} \left[\Psi\left(\frac{\hbar}{4eL_\phi^2 B} + \frac{1}{2}\right) - \ln\left(\frac{\hbar}{4eL_\phi^2 B}\right) \right] \quad (2.5)$$

Where Ψ is the Digamma function, B is the magnetic field and L_ϕ is the phase coherence length, i.e. the length of the path a particle can move without 'losing' its phase. In this formula, α should be $-1/2$ for every band with a π Berry phase [12]. Applying the HLN-formula on the measured conductance at varying magnetic field thus provides a way to

look for surface states.

Recently a study done at MIT has shown that a small correction can be made to the HLN-formula [17]. This addition is quadratic and makes the fit suitable up to higher (greater than 2T) values of the magnetic field. The formula then looks as follows:

$$\Delta\sigma = \frac{\alpha e^2}{h\pi} \left[\Psi\left(\frac{\hbar}{4eL_\phi^2 B} + \frac{1}{2}\right) - \ln\left(\frac{\hbar}{4eL_\phi^2 B}\right) \right] + \beta B^2 \quad (2.6)$$

This additional term is an approximation of the Lorentz deflection. Because of the Lorentz forces the charge carriers experience there is a small B-dependent term in the resistance (and thus also the conductance).

Chapter 3

Experimental Methods

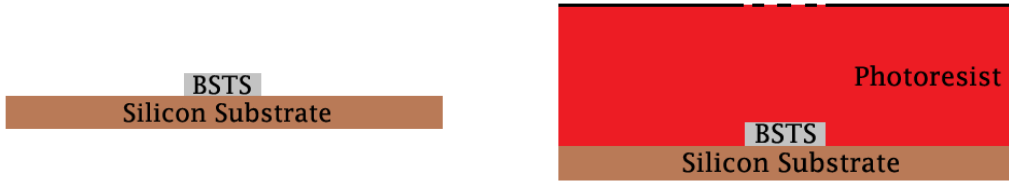
3.1 Sample production

The methods used for producing the samples will be explained briefly in this chapter. The samples that were used are made of bismuth, antimony, tellurium and selenium, often abbreviated to BSTS. This material is a variation of the well-known TI Bi_2Te_3 (bismuth telluride). Some of the bismuth and tellurium has been replaced by antimony and selenide respectively. This replacement is the result of a compromise between bismuth selenium, which is very insulating in the bulk and has a large gap but is unstable, and bismuth telluride, which is less insulating but stable. Of the BSTS crystals, which are grown elsewhere, only extremely thin flakes are required. This can be achieved by exfoliation, commonly called 'the scotch tape method'. By sticking the scotch tape on the BSTS crystal one can peel off thin layers. These can then be rubbed onto a silicon substrate where they will stay due to Van der Waals-bonds. These nanoflakes are typically around 200nm thick [14] [15].

The samples then get coated with a layer of photoresist. The photoresist is sensitive to UV light, so by applying a mask (figure 3.1b) the correct parts of the photoresist can be illuminated making these parts etchable. Removing the photoresist where the gold is required is achieved by chemical etching. the result looks similar to figure 3.2a. Deposition of the gold layer is done by sputtering. (figure 3.2b). After the sputtering the rest of the photoresist is removed by lift off together with the gold that is on top of it. This results in the desired sample configuration. figure 3.2c.

3.2 Measurements

A number of experiments are done to get an understanding of the behavior of BSTS. First of all the basics of BSTS need to be understood. The property of interest here is the resistance. Exact details on the measurements will be provided for each measurement below (measurement 1 and 2). When there is a basic understanding of the BSTS samples, some modifications will be made to the samples. Others have shown that the samples are likely to change their Fermi level over time. This will be tested by repeating



(a) BSTS flake on silicon wafer

(b) sample with photoresist and mask

Figure 3.1: Schematic visualisation of the samples. not to scale

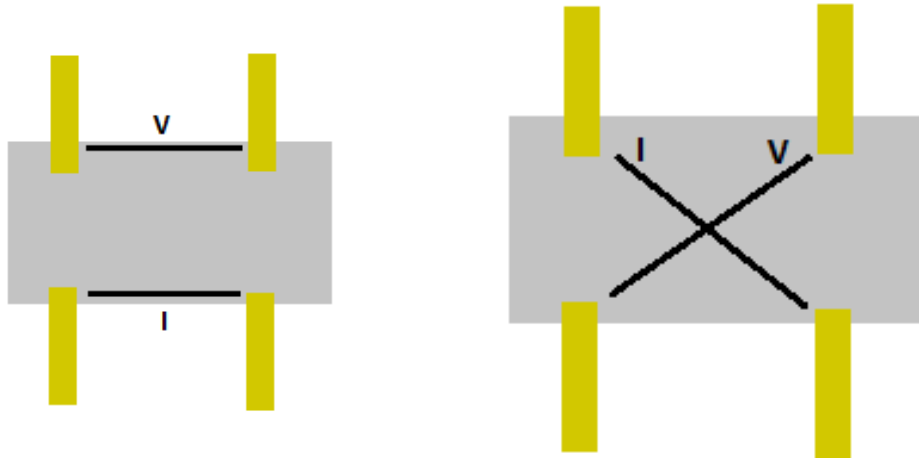


(a) sample after first etching

(b) Sample after gold sputtering

(c) Finished sample

Figure 3.2: Schematic visualisation of the samples. not to scale



(a) Magnetoresistance configuration

(b) Hall resistance configuration

Figure 3.3: PPMS measurements

measurements after a number of days (measurement 3 and 4). We would also like to test the effect of an added Al_2O_3 layer on the surface states in the BSTS (measurement 5).

Sample#1: Control Measurement In order to characterize the BSTS samples and show the existence of surface states several properties of the sample have to be measured. The sample used in this measurement will be referred to as sample#1. The resistance is measured as a function of temperature, ranging from 300K to 2K. This is done both while cooling down and warming up. On the second cooling down the magnetoresistance and Hall resistance are measured. For every set temperature a magnetic field is swept from -3T tot +3T. For these magnetic fields the linear magnetoresistance (figure 3.3a) and the Hall resistance (figure 3.3b) is measured. All of these measurements are done in the same apparatus: the PPMS, Physical Property Measurement System.

To eliminate the contact resistance the measurements of the magnetoresistance are performed with a four-point measurement. The results of the measurement can be found in Chapter 3.2.

Sample #2: Angle resolved This measurement is done in almost the same way as measurement 1. The same PPMS is used to acquire the data. This experiment, however, is conducted on a different sample, sample#2.

Effects that arise because of 2-dimensional sheets in a magnetic field should be affected by the angle that the field makes with the sheet. In other words: If the magnetoresistance that we have measured in measurement 1 is indeed a 2D effect it should be dependent on the angle of the field. For a 3D bulk effect, the angle should not matter. By rotating

the sample inside the PPMS to 0, 20, 40, 60 and 80 degrees a clear cosine dependence in the magnetoresistance and Hall resistance should be visible. All of these measurements are made at a temperature of 12K. The magnetic field is swept from -9K to 9K. The results, again, can be found in chapter 6.

Sample #1 Time dependence After a period of 10 days the sample used in measurement 2, sample#2, is measured again in the PPMS. This time, however, the methods described in measurement 1 are used. So the sample is cooled down to 2K and there is no longer the option of rotating the sample. In this measurement the magnetic field is swept from -9T to 9T to study the effect of the magnetic field on the BSTS more closely.

Changes due to addition of a layer By combining the previously described lift-off method of sample production with PLD (Pulsed Laser Deposition), a 25nm thick layer of Al_2O_3 is placed on top of sample#2. By repeating the experiment described in Measurement 3, the effect is this thin layer on the BSTS surface states can be studied.

Chapter 4

Results

Sample #1: Control Measurement

The measurements performed on BSTS sample 1 are mainly to determine temperature dependence of various characterizing variables. Main interests are hysteresis (the influence of the past on the current state), peak height, carrier density, mobility and fit parameters.

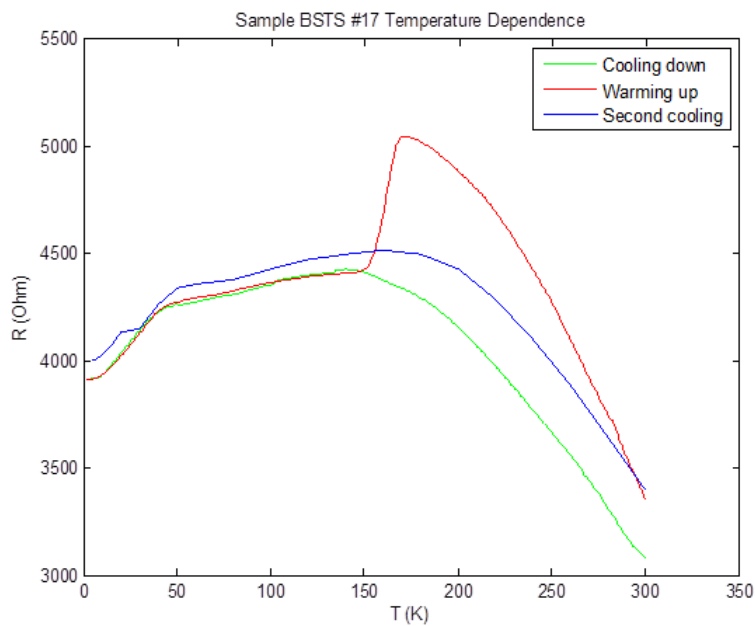


Figure 4.1: RT-curves of cooling the sample down (green), warming it up (red), and cooling it down again (blue)

The sample shows hysteresis when warmed up, but the cooling down curves show clear resemblance. It is therefore important to be consistent with measurements; all of

our measurements are performed the during cooling down of the sample. The cause of this hysteresis in resistance may be some dust or other particles (most likely CO_2 -particles, since its boiling point is in the region of large hysteresis) which act as doping and thus lower resistance. It is possible this impurity is cleaned from the sample at lower temperatures. When the bulk states of the sample start to matter, the sudden lack of doping would show up in the data is a heightened resistance. In due time most of the contamination returns to the sample, which is why the second cooling curve is very similar to the first. It is probably only during the warming up stage that hysteresis is influential.

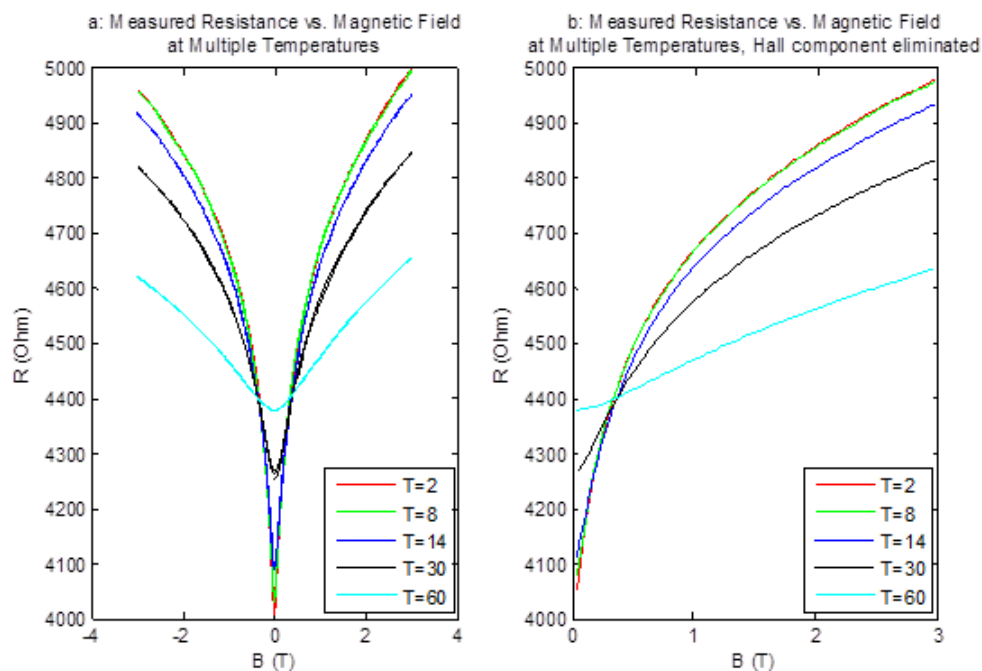


Figure 4.2: Measured resistance of BSTS vs. magnetic field, at multiple temperatures (a) and measured resistance of BSTS vs. magnetic field, at multiple temperatures and eliminated Hall component (b)

Measurement of the resistance shows the expected downwards peak due to antilocalization. The peak height shows clear temperature dependence. This is consistent with the expectation that weak antilocalization is insignificant at higher temperatures. Although the measurements were performed over the horizontal bridge, a small Hall component was inevitably picked up. To eliminate this Hall component, the average has been taken between the negative and the positive magnetic field branch, the result of which are shown in figure 4.2(b). The dependence of the peak height on temperature is shown in figure 4.3. It is clearly not linear. The dependence is strongest at low temperatures, and quite stable at higher temperatures.

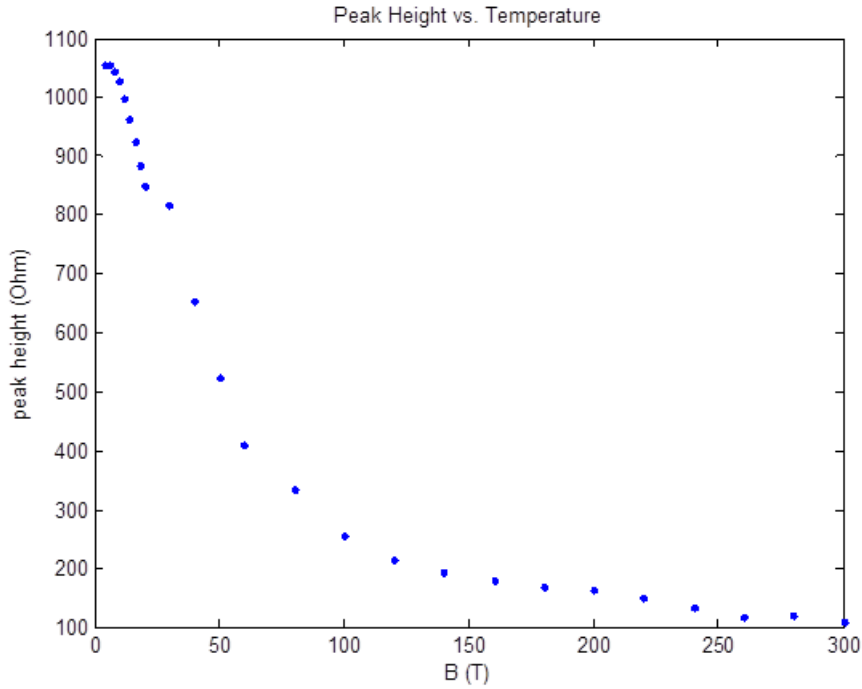


Figure 4.3: Temperature dependence of the peak height

Hall measurement From the raw data (figure 4.4) the Hall component is already clearly visible. Isolation is performed by subtracting the positive magnetic field branch from the negative. When the Hall component is isolated, the slope remains unaltered until much higher temperatures. This is reflected in a relatively stable carrier density at lower temperatures

Though some variation occurs, the carrier density does not change a lot until temperatures as high as 180 K. From the carrier density and the resistance, the mobility can be calculated using:

$$\mu = \frac{I}{n_s V_x \frac{W}{L}} \quad (4.1)$$

Carrier density and mobility are plotted in figure 4.5.

To determine the dimensionality of states in the sample, it is necessary to determine the fitting parameter α in the Higami-Larkin-Nagaoka formula:

$$\Delta\sigma = \frac{\alpha e^2}{h\pi} \left[\Psi\left(\frac{\hbar}{4eL_\phi^2 B} + \frac{1}{2}\right) - \ln\left(\frac{\hbar}{4eL_\phi^2 B}\right) \right] \quad (4.2)$$

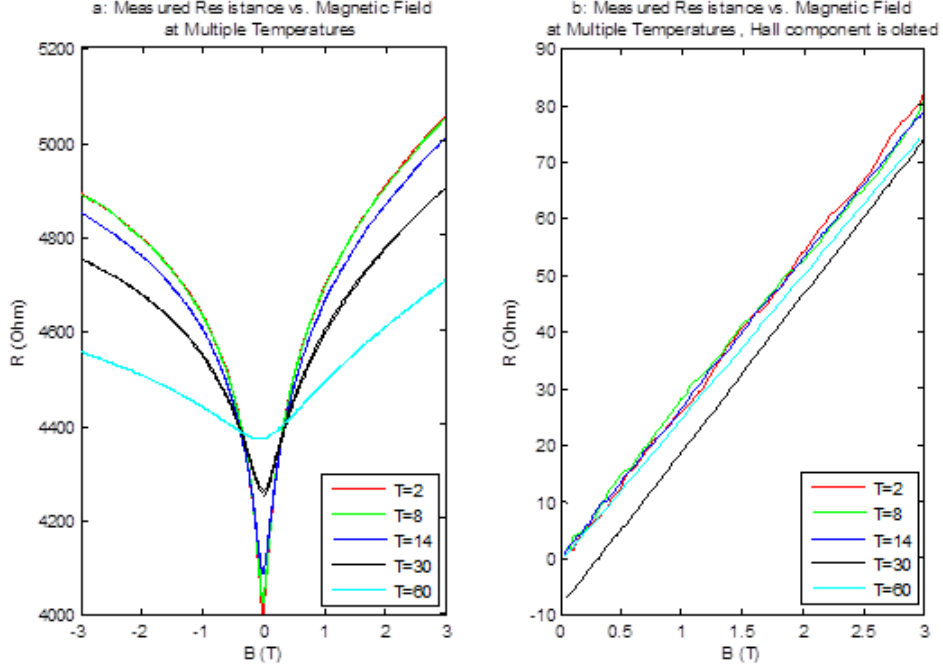


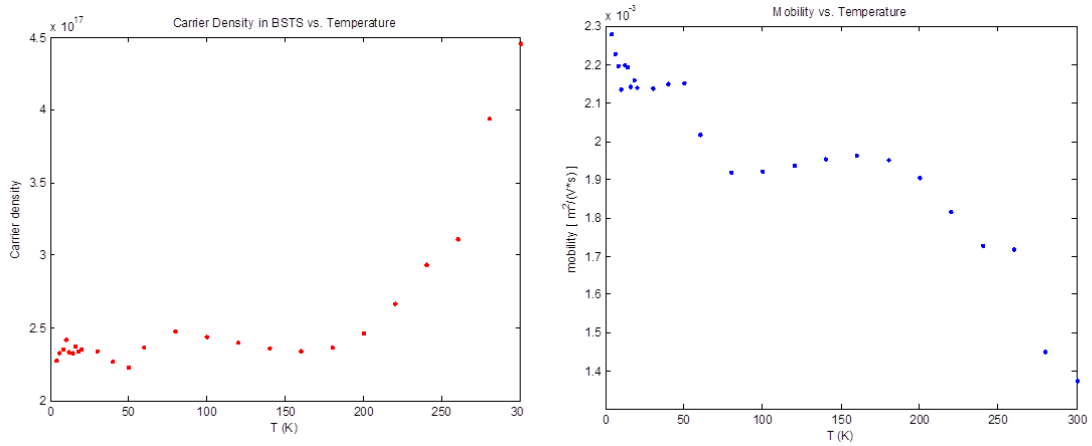
Figure 4.4: Hall measurement data (a) and Hall resistance vs. magnetic field (b)

As described in Theoretical Aspects, for a single 2D state a value of -0.5 is expected for α . L_ϕ is expected to be in the order of nanometers. The fitting procedure involves looping over various values for α and the phase coherence length, calculating the Mean-Square Error of the fit, and selecting the lowest error achieved.

Phase Coherence Length and the fitting parameter α are plotted in figure 4.7. The phase coherence length seems to decrease linearly with rising temperature. A decrease in phase coherence length is expected, as the amount of inelastic scattering events should raise with higher temperature.

A slight decrease in α is observed as temperature rises. Only a small influence was expected; at sufficiently low temperatures variation in temperature should not have too much effect on the dimensionality of the states.

The found value of α is significantly lower than the expected -0.5 . Lu and Shen [12] remark that in practice the calculated value for α usually lies in the interval -0.4 to -1.1 , sometimes as far -1.5 . This is a result from multiple bands contributing to the value of α . Notably the other large surface of the sample, the downside touching the substrate, can theoretically push α to -1 . In addition it is theorized that coupling in the crystal is not as strong in the direction orthogonal to the surface as in the plane of the surface. Because of strong spin-orbit coupling in the bulk, the bulk also contributes to the value of α . Therefore the found values of α , around -1.25 , indicate the presence of 2D states.



(a) Carrier density in BSTS sample 1 at various temperatures
 (b) Dependence of the mobility in the sample at various temperatures

Figure 4.5: Carrier density and mobility

Sample #2: Angle resolved

Figure 4.8 shows the linear magnetoresistance for 5 different angles of the external magnetic field. The correction for the Hall resistance is the same as for sample#1. The WAL peak is clearly visible in this graph (because resistance is plotted instead of conductance the peak points downward). Even though the angles are linearly chosen, the graphs appear to move further apart. This behaviour is more closely studied in the two following graphs.

The data from the previous figure is now plotted against $B \cos(\theta)$ instead of just the magnetic field (figure 4.9a). The graphs now are now perfectly aligned! One would expect that 2D structures are dependent of the angle of the magnetic field, whereas 3D structures should not be dependent of the angle at all. This graph shows a nearly perfect cosine dependence on the magnetic field, which clearly indicates a two dimensional behavior of the sample. This is also shown by [14].

Figure 4.8 showed hints of cosine dependence in the spacing of the different graphs. In figure 4.9b the peak height is defined as the difference between the highest and lowest part of the graph. These peak heights are then normalized. The cosine function is fitted by estimating the value of $\cos(1/2\pi)$ by extrapolating the data. The optimal fit is shown in the figure. From this graph it is clear that the graphs indeed shift as a function of the angle of the magnetic field. Together with figure 4.9a, this is a clear indication for the two dimensional behaviour of the BSTS samples. Figure 4.10a shows the data

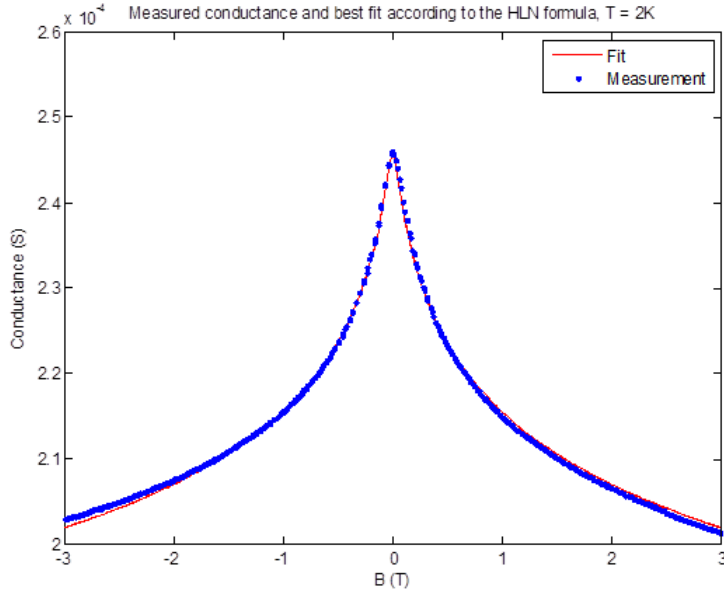
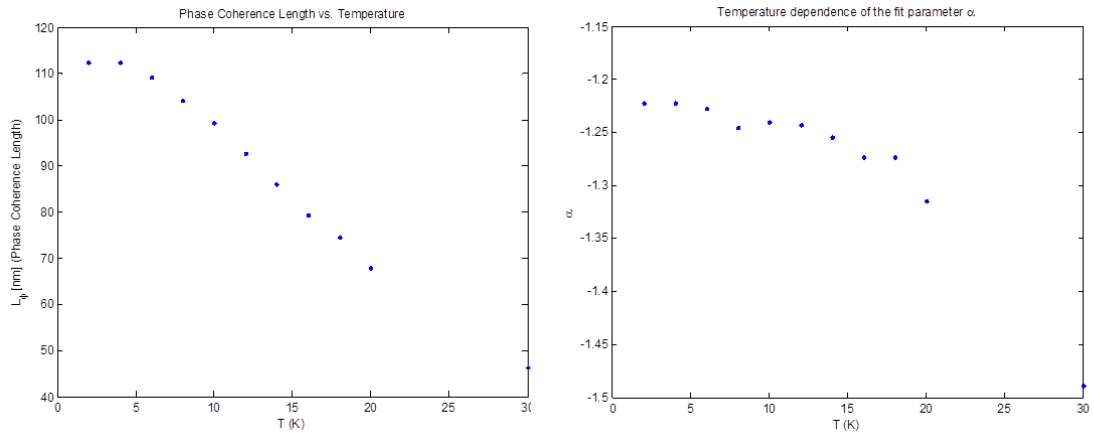


Figure 4.6: An example of a fit to the measured conductance (Hall component not yet eliminated) using the HLN-formula. The found fitting parameters in this example are: $\alpha = -1.0450$, $L_\phi = 107.58$ nm

measured by the PPMS in blue after it has been corrected for the Hall component. The red dataset shows the best possible fit for the entire graph. The two fitting parameters for the fit shown figure 4.10a are: $\alpha = -2.716 \pm 0.4$ and $l_\phi = 122.4 \pm 18$ nm. The error is calculated by limiting what fits are still acceptable, although worse than the fit shown in the figure. The value of l_ϕ , 122.4nm is a realistic one. For temperatures as low as 12K the phase coherence length will not be extremely large. Also, the phase is not lost on every collision. The value of l_ϕ thus supports the validity of the measurements and the fit. The fitting parameter, α , is somewhat larger than generally expected. As mentioned before, $-1/2$ is expected for a single surface state. -2.7 would thus indicate at least 5 surface states, which is impossible for a, nearly, two dimensional device. There are several ways of explaining this rather large value of α . First and foremost, the fit of 4.10a does not seem to fit the data all that well. Fitting with the beta correction for example, provides a much better fit and also gives rise to a different fitting parameter. The second explanation has been mentioned earlier for measurement 1. The bulk states in the sample may be contributing to the 2D conductance, because of weak coupling between two layers in the sample. Although they are not surface states, the bulk states still contribute to the 2D conductance in that case. Because of the differences between the actual data and the first, the first explanation appears to be the most accurate and will be examined further.

A way of improving the fit in figure 4.10a is by adding an extra quadratic term to bend the fit into a straight line at higher magnetic fields. For more information on this,



(a) Temperature dependence of the determined phase coherence length (b) Temperature dependence of the fit parameter α

Figure 4.7: Fitting parameters of the HLN-formula

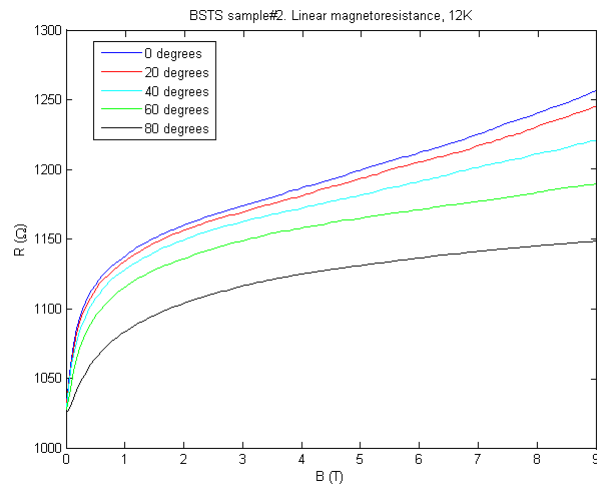
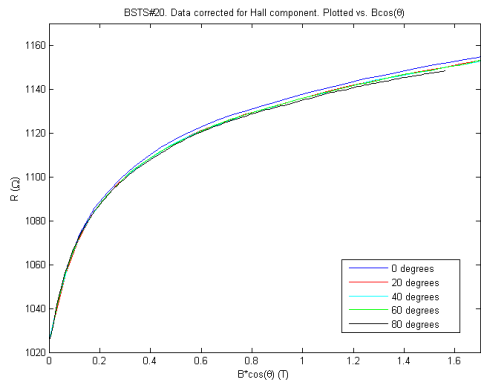
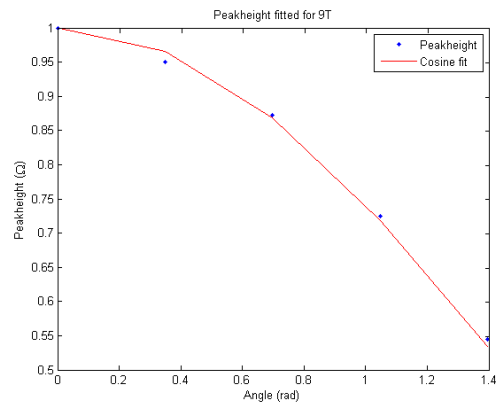


Figure 4.8: sample#2. Measured at 12K, rotating B-field, raw magnetoresistance

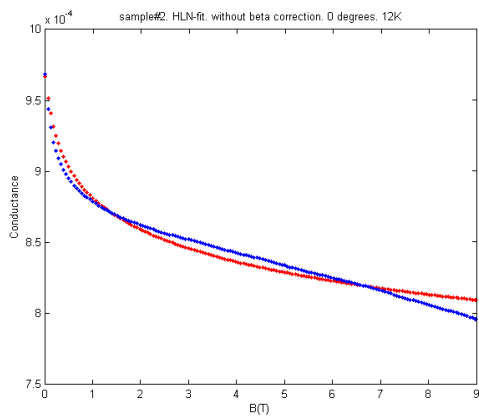


(a) 12K, Bcos plotted

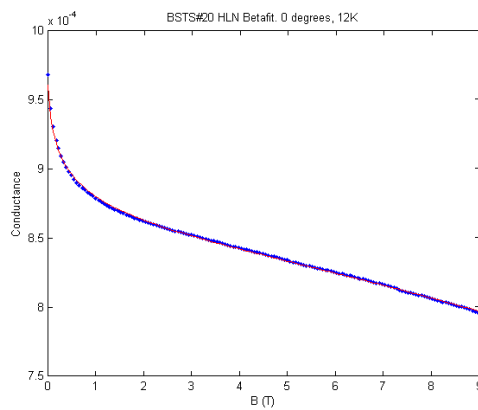


(b) 12K, peak heights

Figure 4.9: Angle Resolved measurement data



(a) sample#2. 12K, rotating B-field. HLNfit



(b) sample#2. 12K rotating B. HLNfit betacorrected

Figure 4.10: Measurement2, fits

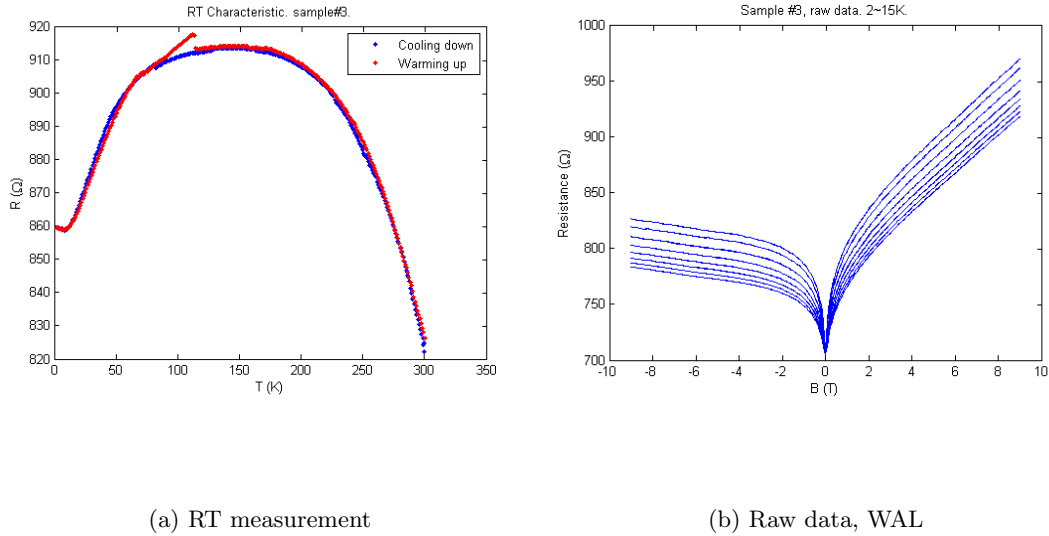


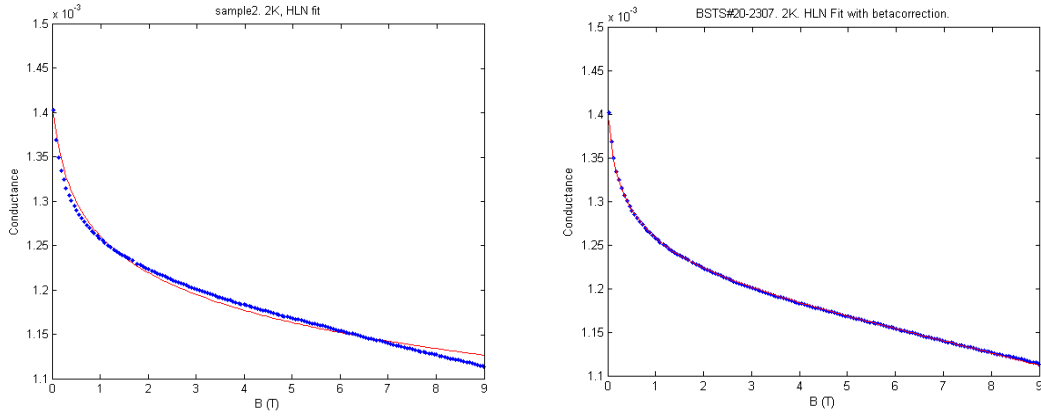
Figure 4.11: measurement3,Raw data

please see chapter 4.3. The data (blue) shown in the graph above is the same as in figure 4.10a. The fit, however, has improved dramatically. A new fit, of course, has new fitting parameters. This time there is also a β fitting parameter. The phase coherence length is now $222.5 \pm 20\text{nm}$. Fitting parameter α for this fit is -1.896 ± 0.1 . The β parameter is $-4.03 \times 10^{-7} \mu\text{S}/\text{T}^2$. Fitting parameter α is now around -1.9 instead of -2.7. This value is more in line with the expected value for the sample. The phase coherence length, although larger than in the previous fit, is an acceptable value. Together with the fact that the fit looks very good, this means that the fit shown in figure 4.10b is better than in figure 4.10a. $\alpha = -1.89$ is therefore more credible than -2.7.

Sample #1 Time Dependence

Figure 4.11 shows the raw data of measurement 3. In 4.11a the RT graph is displayed. There is a lot less hysteresis than in the measurement of sample#1 (measurement 1). Although there is still a small peak visible in the warming up part of the graph, it can be concluded from this that the sample and atmosphere are much cleaner in this measurement. Figure 4.11b shows the raw data of the magnetic field sweep for temperatures between 2 and 15 K. The graph illustrates that the peak gets sharper and deeper the colder the sample is. At lower temperatures the phase coherence length is longer and therefore the Weak antilocalization is stronger. This is illustrated by the deeper peaks.

An important method of determining the presence of 2D conductance is the Hikami, Larkin, Nagaoka fit. In figure 4.12 the data from the measurements is fitted with the



(a) HLN Fit

(b) HLN Fit with correction

Figure 4.12: measurement 3, Fits

basic HLN function (4.12a) and the HLN fit with quadratic correction (4.12b). The corrected HLN function fits the measurements much better than the original HLN function, as can be seen in the graphs. The two fits produced are made using the following parameters:

For the basic HLN fit:

$$\alpha = -5.114 \pm 1.38$$

$$l_\phi = 100.9 \pm 83 \text{ nm}$$

And for the corrected HLN fit:

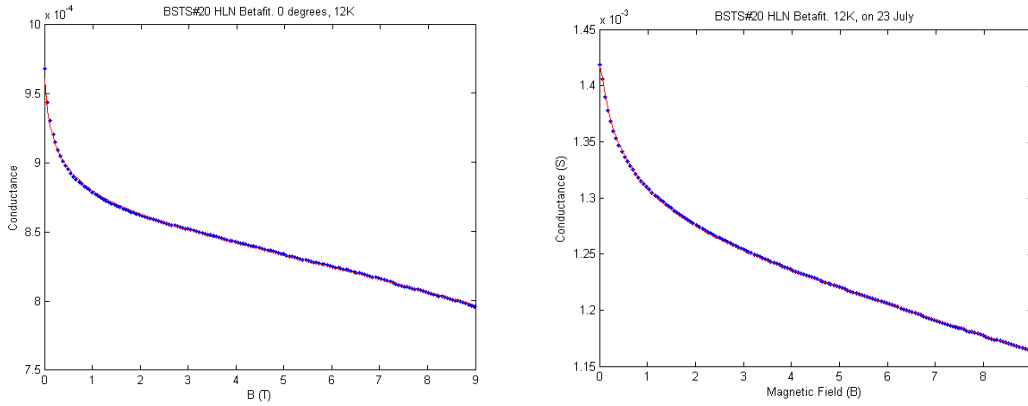
$$\alpha = -3.9910 \pm 1.3$$

$$l_\phi = 143.9 \pm 22 \text{ nm}$$

$$\beta = -5 \times 10^{-7} \pm 5 \times 10^{-8}$$

Both fits produce acceptable values for the phase coherence length, but differ greatly in the value of α . A single surface state should contribute $-1/2$ to this fitting parameter. The corrected HLN fit, which also fits the data best, thus provides a value for α that is better in line with expectations. -3.99 still implies the presence of eight "surface" states. It is most likely that bulk states are contributing to the conductance. When these bulk states have a 2D behavior they will show up in the fitting parameter α .

Comparison A possibly interesting feature of BSTS is that its electrical properties may change over time. The cause of this is still unknown, but after 10 days the measurements do show some changes. The conductance seems to have increased over time. This



(a) HLN Betafit measurement2

(b) HLN Betafit measurement 3

Figure 4.13: measurement 3, Fits

is visible in the data when 4.8 is compared with 4.11. The average resistances lowers from 1150 to 860 Ohms.

The parameters corresponding with the best possible HLN fit also change, as is illustrated in 4.13

The values of α and l_ϕ thus also change over time. α has changed from -1.896 ± 0.1 to -4.018 ± 0.36 over the course of 10 days. l_ϕ has changed from $222.5 \pm 20\text{nm}$ to $99.3 \pm 15.5 \text{ nm}$! The samples change quite a lot in a matter of 10 days. It would seem that the desired properties of a TI get less and less over time. That is, the bulk conductance increases relative to the surface conductance.

Another way of looking into the bulk conductance versus the surface conductance is by determining the energy at which the state occurs. A surface state in a TI will typically be found in the bandgap (a key feature of the TI). If the state is outside of the bandgap, this indicates more bulk conductance. From the charge carrier density the energy can be calculated through:

$$k_f = \sqrt{2\pi n_s} \quad (4.3)$$

$$E = \hbar\nu k_f \quad (4.4)$$

Where n_s is the charge carrier density and $\nu = 4.6 \cdot 10^5 \text{ m/s}$. The charge carrier density can be found in the Hall data.

The typical bandgap for $\text{Bi}_{1.5}\text{Sb}_{0.5}\text{Te}_{1.8}\text{Se}_{1.2}$ is 0.3 eV [18]. For the first measurement of sample#2 (i.e. the angle resolved measurement) the calculated energy is 0.448 eV. This shows that the conducting state is outside of the bandgap and that some bulk

conductance may show in the measurements. From discussion with the UvA (producer of the samples) it can be concluded that this energy of 0.448 eV can still be in the bandgap [19]. The charge carriers behave two-dimensionally, so that there is no need to correct for the thickness of the sample. The measured conductance is most likely generated by the surfaces of the sample.

When the energy is calculated for the measurement 10 days later, a value of 0.391 eV is found. This is still outside of the bandgap albeit closer to the bandgap. This shifting of the energy over time is an interesting behavior of the BSTS sample. It would be most interesting and useful if this shift in energy will continue into the bandgap. The energy where the surface state is found, can then be controlled!

Changes due to addition of a layer

The PPMS measurements of sample#2 with a thick layer of Al_2O_3 have turned out to produce nearly infinite resistance. This, of course, means that there is no conductance between two contacts. Under a microscope it is visible that after a full day of etching in acetone nearly all photoresist is still on the sample. This thick layer of photoresist is most likely blocking the current from the bonds to the gold contacts. From these measurements we can only conclude that using lift-off to grow Al_2O_3 layers on BSTS is not a usable method. A possible explanation for that fact that the photoresist does not etch off, is that the heat from the PLD plasma has baked the photoresist too much. Even though no sample heating was used during the PLD, the atoms that hit the sample may have had too much energy to leave the photoresist untouched.

Due to this thick layer of photoresist no contact could be made between the gold and the measurement system. A better way of producing the required samples for this measurement, is first growing the Al_2O_3 layer directly on top of the BSTS flake and the gold. Then the parts of the Al_2O_3 that are unnecessary can be etched away. Gold does etch a lot faster than the insulating Al_2O_3 . The gold contacts, however, are approximately five times thicker than the Al_2O_3 layer (125 and 25nm respectively), which leaves a margin of error in the etch time and speed. We are confident that this method of production will produce nice and usable samples.

Chapter 5

Conclusions

The main interest of this research was the applicability of BSTS as a topological insulator with low conductance in the bulk and high conductance of the surface. To determine this we will first draw conclusions from the separate measurements.

Sample #1: Control Measurement

In this measurement several properties of BSTS were determined. Important conclusions are:

- The resistance of BSTS shows clear hysteresis in response to varying temperature. The exact cause for this is uncertain, but it is suspected some contamination of the sample is altering the conductance during the cooling down of the sample.
- There is weak antilocalization present in BSTS, and fitting it to the HLN-formula produces values expected for 2D surface states. Carrier density is relatively constant at low temperatures (below 150 K)

Sample #2: Angle resolved

To further analyze the dimensionality of the system, measurements along multiple angles were performed.

- There is clear dependence of the resistance on the angle. The relation can be accurately described by a cosine relation. Because only 2D states should depend on angle, the current through BSTS is two dimensional.
- Adding the quadratic term to the HLN-formula drastically improves the fit of the data, especially at higher magnetic field

- The found values of the fitting parameter α show there are more contributions to conductance than just the surface states; a very likely influence is the contribution of bulk conductance behaving somewhat two dimensional.

Sample #1 Time Dependence

The main goal of this measurement session was to determine the alteration of properties of the sample over time.

- The conductance shows a clear increase of about 4 mS over a course of 10 days. In conclusion, alteration of the sample over time on some scale is definitely existent.

Changes due to addition of a layer

Although no actual results have been produced, a definite conclusion can be drawn regarding production methodology. Lift-off is not a suitable way to grow Al₂O₃ on BSTS. A better production method is simply to grow Al₂O₃ directly onto the sample and use careful etching to remove the unnecessary.

Final conclusions

The presence of 2D states is considered proven. Angle dependence, weak antilocalization results and the two-dimensional behavior of the charge carriers, indicate 2D current in BSTS. The angle dependence and behavior of the charge carriers strongly indicate the presence of surface states. However, the results from the weak antilocalization experiments also indicate the possibility of bulk conductance. This can be problematic for future experiments elaborating on the unique properties of a quantum spin hall state. There are even more difficulties to be overcome if BSTS is to be used in other experiments. Resistance shows clear hysteresis in response to varying temperature, and BSTS behaves differently over time. On the other hand, surface current is existent. If it is possible to isolate the 2D surface states, BSTS might prove itself to be immensely valuable in the search for some exotic particles.

Bibliography

- [1] Konig et al. *Quantum Spin Hall Insulator State in HgTe Quantum Wells*, Science 317, pg 766, 2007
- [2] M.Z. Hasan, C.L. Kane *Topological Insulators*, Rev.Mod.Phys. 82:3045, 2010
- [3] D. Griffiths, *Introduction to Quantum Mechanics*, 2nd edition, Pearson education international, 2005
- [4] X.L.Qi, S.C. Zhang *Topological Insulators and Superconductors*, Reviews of Modern Physics, 83, pg 1058, 2011
- [5] Ashcroft/Mermin, *Solid State Physics*. Brooks/Cole, Belmont, CA. 1976
- [6] S. Datta, *Electronic Transport in Mesoscopic Systems*, Cambridge University Press, Cambridge, 1995
- [7] C. Kittel, *Introduction to Solid State Physics*, John Wiley & Sons Inc., 1996
- [8] M. Veldhorst, M. Snelder, M. Hoek, T. Gang, X.L. Wang, V. K Guduru, U. Zeitler, W.G. v.d. Wiel, A.A. Golubov, H. Hilgenkamp, A. Brinkman, *Josephson supercurrent through a topological insulator surface state*, Nature Materials 11, 417, 2012
- [9] V.F. Gantmakher, *Electrons and Disorder in Solids*, Oxford University Press 2005, 1st edition
- [10] M. Snelder, A. Brinkman, *Topologische isolatoren, oppervlakkig bekeken*, Nederlands Tijdschrift voor Natuurkunde, February 2012
- [11] S. Hikami, A.I. Larkin, Y. Nagaoka, *Spin-Orbit Interaction and Magnetoresistance in the Two Dimensional Random System Prog. Theor., Phys.* vol. 63, No.2., February 1980
- [12] H. Lu, S. Shen, *Weak localization of bulk channels in topological insulator thin films*, Physical Review B84, 125138, 2011
- [13] X.L. Qi, S.C. Zhang, *The quantum spin Hall effect and topological insulators*, Physics today, january 2010, pg 33.

- [14] B. Xia, P. Ren, A. Sulaev, S. Chen, C. Soci, X. Yu, H. Ou, A. Huan, A.T.S. Wee, A. Rusydi, S.Q. Shen, L. Wang, *Significant surface transport in topological insulator $Bi_{1.5}Sb_{0.5}Te_{1.8}Se_{1.2}$ single crystalline nanoflake device* <http://arxiv.org/abs/1203.2997>, visited 18/07/2012
- [15] D. Teweldebrhan, V. Goyal, A.A. Balandin, *From Graphene to Bismuth Telluride: Mechanical Exfoliation of Quasi-2D Crystals for Applications in Thermoelectrics and Topological Insulators*, Nano Lett. 10, 1209, 2010
- [16] H. Zhang, C.X. Liu, X.L. Qi, X. Dai, Z. Fang, S.C. Zhang, *Topological insulators in Bi_2Se_3 , Bi_2Te_3 and Sb_2Te_3 with a single Dirac cone on the surface*, Nature physics, 2009. DOI: 10.1038/NPHYS1270
- [17] B. Assaf, T. Cardinal, P. Wei, F. Katmis, J. Moodera, D. Heiman, *Linear magnetoresistance in topological insulators: Quantum phase coherence effects at high temperatures*, unpublished
- [18] T. Arakane, T. Sato, S. Souma, K. Kosaka, K. Nakayama, M. Komatsu, T. Takahashi, Z. Ren, K. Segawa, Y. Ando, *Tunable Dirac cone in the topological insulator $Bi_{2-x}Sb_xTe_{3-y}Se_y$* , Nature communications, 2012, DOI: 10.1038/ncomms1639
- [19] Private communications with University of Amsterdam